Inorganic Chemistry
Article

*Inorg. Chem.* **2009**, *48*, 9861–9873 **9861**
DOI: 10.1021/ic9014916

# Discovering the Complex Chemistry of a Simple $Ni^{II}/H_3L$ System: Magnetostructural Characterization and DFT Calculations of Di- and Polynuclear Nickel(II) Compounds

**Matilde Fondo,*,† Noelia Ocampo,† Ana M. García-Deibe,† Eliseo Ruíz,‡ Javier Tercero,‡ and Jesús Sanmartín§**

†*Departamento de Química Inorgánica, Facultade de Ciencias, Universidade de Santiago de Compostela, 27002 Lugo, Spain,* ‡*Departament de Química Inorgànica, Institut de Química Teórica i Computacional, and Institució Catalana de Recerca i Estudis Avançats, Universitat de Barcelona, Diagonal 647, 08028 Barcelona, Spain, and* §*Departamento de Química Inorgánica, Facultade de Química, Universidade de Santiago de Compostela, 15782 Santiago de Compostela, Spain*

Received July 27, 2009

The simple nickel(II) acetate/$H_3L$ system ($H_3L$ = 2-(2-hydroxyphenyl)-1,3-bis[4-(2-hydroxyphenyl)-3-azabut-3-enyl]-1,3-imidazolidine) presents an unusually complicated reactivity scheme, which strongly depends on the $Ni(OAc)_2/H_3L$ molar ratio and on the pH of the medium. Thus, in addition to the formerly reported compounds $[Ni_2L(OAc)(H_2O)_2][Ni_2L(OAc)(H_2O)(HOAc)]\cdot 3.25H_2O$, **1**$\cdot 3.25H_2O$; $[\{Ni_3L(OAc)(OH)(H_2O)(MeOH)_2\}(CO_3)\{Ni_2L(OAc)(MeOH)_2\}]\cdot 2.7H_2O\cdot 1.5MeOH$, **2**$\cdot 2.7H_2O\cdot 1.5MeOH$; and $[Ni_3L(OAc)_2(OH)(H_2O)(MeOH)_2]\cdot 3H_2O\cdot 0.5MeOH$, **3**$\cdot 3H_2O\cdot 0.5MeOH$, this system can also yield some other complexes as $[Ni_2L(o\text{-}O{-}C_6H_4{-}CHO)(H_2O)]\cdot 1.75H_2O$, **4**$\cdot 1.75H_2O$; $[Ni_2L(OH)(H_2O)(MeOH)]\cdot 3H_2O\cdot 1.5MeOH$, **5**$\cdot 3H_2O\cdot 1.5MeOH$; $[Ni_2L(OAc)(MeOH)_2]\cdot H_2O\cdot 3MeOH$, **6**$\cdot H_2O\cdot 3MeOH$; and $[\{Ni_2L(MeOH)\}(CO_3)\{Ni_2L(MeOH)_2\}]\cdot 4.75H_2O\cdot 2MeOH$, **7**$\cdot 4.75H_2O\cdot 2MeOH$. A detailed study of the reaction scheme that allows obtaining all of these complexes is presented herein, as well as the structural characterization of the novel compounds **4**$\cdot 1.75H_2O$ to **7**$\cdot 4.75H_2O\cdot 2MeOH$. X-ray analyses show that all of them present stereoisomery in the solid state. In this way, **6**$\cdot H_2O\cdot 3MeOH$ appears particularly interesting, as its molecular and supramolecular chirality is only controlled by hydrogen bonds. Magnetic studies of **5**$\cdot 3H_2O$ to **7**$\cdot 4.75H_2O\cdot 2MeOH$ are also discussed, and the complicated magnetic superexchange pathway shown by **7**$\cdot 4.75H_2O\cdot 2MeOH$ is analyzed in light of DFT calculations.

## Introduction

The coordination chemistry of 2-(2-hydroxyphenyl)-1,3-bis[4-(2-hydroxyphenyl)-3-azabut-3-enyl]-1,3-imidazolidine ($H_3L$, Chart 1) and homologous ligands shows that they almost invariable behave as dicompartmental donors when they bind to first row d-block cations[1−7] or p-block metals[8] and that they give rise to $M_2L_2$ sandwich compounds when M is a lanthanide cation.[9−11] Thus, the chemistry of $H_3L$

*To whom correspondence should be addressed. E-mail: matilde.fondo@usc.es.

(1) Bailey, N. A.; Mckenzie, E. D.; Worthington, J. M. *Inorg. Chim. Acta* **1977**, *25*, L137–L138.
(2) Chiari, B.; Piovesana, O.; Tarantelli, T.; Zanazzi, P. F. *Inorg. Chem.* **1983**, *22*, 2781–2784.
(3) (a) Mukhopadhyay, V.; Govindasamy, L.; Ravikumar, K.; Vehmurugan, D; Ray, D. *Inorg. Chem. Commun.* **1998**, *1*, 152–154. (b) Bera, M.; Wong, W. T.; Aromí, G.; Ray, D. *Eur. J. Inorg. Chem.* **2005**, 2526–2535. (c) Paital, A. R.; Mikuriya, M.; Ray, D. *Eur. J. Inorg. Chem.* **2007**, 5360–5369.
(4) Copeland, P.; Kahwa, I. A.; Mague, J. T.; McPherson, G. L. *J. Chem. Soc., Dalton Trans.* **1997**, 2849–2852.
(5) (a) Fondo, M.; García-Deibe, A. M.; Sanmartín, J.; Bermejo, M. R.; Lezama, L.; Rojo, T. *Eur. J. Inorg. Chem.* **2003**, 3703–3706. (b) Fondo, M.; García-Deibe, A. M.; Corbella, M.; Ribas, J.; Llamas-Saiz, A. L.; Bermejo, M. R.; Sanmartín, J. *Dalton Trans.* **2004**, 3503–3507. (c) Fondo, M.; Ocampo, N.; García-Deibe, A. M.; Corbella, M.; Bermejo, M. R.; Sanmartín, J. *Dalton Trans.* **2005**, 3785–3794. (d) Fondo, M.; García-Deibe, A. M.; Ocampo, N.; Sanmartín, J.; Bermejo, M. R.; Llamas-Saiz, A. L *Dalton Trans.* **2006**, 4260–4270. (e) Fondo, M.; Ocampo, N.; García-Deibe, A. M.; Corbella, M.; El Fallah, M. S.; Cano, J.; Sanmartín, J.; Bermejo, M. R. *Dalton Trans.* **2006**, 4905–4913.
(6) (a) Fondo, M.; García-Deibe, A. M.; Bermejo, M. R.; Sanmartín, J.; Llamas-Saiz, A. L. *J. Chem. Soc., Dalton Trans.* **2002**, 4746–4750. (b) Fondo, M.; García-Deibe, A. M.; Ocampo, N.; Bermejo, M. R.; Sanmartín, J. *Dalton Trans.* **2004**, 2135–2141. (c) Fondo, M.; García-Deibe, A. M.; Corbella, M.; Ruiz, E.; Tercero, J.; Sanmartín, J.; Bermejo, M. R. *Inorg. Chem.* **2005**, *44*, 5011–5020. (d) Fondo, M.; Ocampo, N.; García-Deibe, A. M.; Vicente, R.; Corbella, M.; Bermejo, M. R.; Sanmartín, J. *Inorg. Chem.* **2006**, *45*, 255–262. (e) Fondo, M.; García-Deibe, A. M.; Ocampo, N.; Sanmartín, J.; Bermejo, M. R.; Oliveira, E.; Lodeiro, C. *New J. Chem.* **2008**, *32*, 247–257.
(7) (a) Nanda, P. K.; Aromí, G.; Ray, D. *Chem. Commun.* **2006**, 3181–3182. (b) Paital, A. R.; Hong, C. S.; Kim, H. C.; Ray, D. *Eur. J. Inorg. Chem.* **2007**, 1644–1653. (c) Paital, A. R.; Tak Wong, W.; Aromí, G.; Ray, D. *Inorg. Chem.* **2007**, *46*, 5727–5733. (d) Paital, A. R.; Bertolasi, V.; Aromí, G.; Ribas-Ariño, J.; Ray, D. *Dalton Trans.* **2008**, 861–864.
(8) Wei, P.; Atwood, D. *J. Chem. Soc., Chem. Commun.* **1997**, 1427–1428.
(9) Isobe, T.; Kida, S.; Misumi, S. *Bull. Chem. Soc. Jpn.* **1967**, *40*, 1862–1863.
(10) Howell, R. C.; Spence, K. V. N.; Kahwa, I. A.; Williams, D. J. *J. Chem. Soc., Dalton Trans.* **1998**, 2727–2734.
(11) Yang, L. W.; Liu, S.; Wong, E.; Rettig, S. J.; Orvig, C. *Inorg. Chem.* **1995**, *34*, 2164–2178.


Published on Web 09/17/2009

**Chart 1**

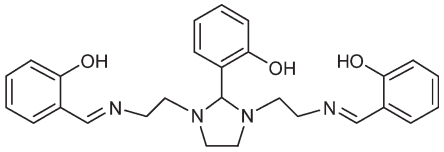


appears to be rather predictable, albeit the unforeseen properties and structural features of some of its compounds, and the studies performed by others and us,[1−8] allow an inferrence to be made regarding some patterns. Accordingly, if lanthanide metals are excluded, all of the complexes containing this ligand are either binuclear $M_2LX_n$ species ($n$ depending on the metal oxidation state and on the anionic charge of the exogenous ligand X)[1−5,8] or tetranuclear clusters based on the $[M_2L]^+$ block, with different connectors.[6,7] To the best of our knowledge, there is only one exception to this rule, which has been reported by us,[12] where $H_3L$ acts in a trinucleating fashion.

In this way, we have recently described[12] that the interaction of $Ni(OAc)_2$ with $H_3L$ clearly diverges from the expected behavior and that, under different conditions, it can yield a quite unusual binuclear complex ($[Ni_2L(OAc)(H_2O)_2][Ni_2L(OAc)(H_2O)(HOAc)]\cdot 3.25H_2O$, $\mathbf{1}\cdot 3.25H_2O$), an astonishing asymmetric pentanuclear cluster ($[\{Ni_3L(OAc)(OH)(H_2O)(MeOH)_2\}(CO_3)\{Ni_2L(OAc)(MeOH)_2\}]\cdot 2.7H_2O\cdot 1.5MeOH$, $\mathbf{2}\cdot 2.7H_2O\cdot 1.5MeOH$), or an also unexpected trinuclear compound ($[Ni_3L(OAc)_2(OH)(H_2O)(MeOH)_2]\cdot 3H_2O\cdot 0.5MeOH$, $\mathbf{3}\cdot 3H_2O\cdot 0.5MeOH$), where both **2** and **3** are examples of the trinucleating ability of $H_3L$ (Figure 1). Therefore, it seems that, in this particular case, the chemistry of $H_3L$ is rather singular and that the simple $Ni(OAc)_2/H_3L$ system is the base of a reaction scheme more complicated than that foreseeable in principle. Consequently, in an attempt to understand the chemistry involved in these unexpected and apparently serendipitous finds, we persevered with the study of the reactivity of the nickel(II) acetate/$H_3L$ system, in the hope of rationalizing the isolation of asymmetric binuclear, trinuclear, and pentanuclear complexes, in contrast with other more symmetric binuclear and tetranuclear compounds. The results obtained, with a rigorous analysis of the magnetic properties of the novel isolated complexes, are described herein.

## Experimental Section

**General Considerations.** Elemental analyses of C, H, and N were performed on a Carlo Erba EA 1108 analyzer. Infrared spectra were recorded as KBr pellets on a FT-IR Bruker IFS-66v spectrophotometer in the range 4000−400 $cm^{-1}$. Electrospray mass spectra of the metal complexes were obtained on a Hewlett-Packard LC/MS spectrometer, in methanol as the solvent.

**Syntheses.** All solvents and $NMe_4OH\cdot 5H_2O$ are commercially available and were used without further purification. Complex $\mathbf{1}\cdot 3.25H_2O$ was obtained as previously reported[12] and satisfactorily characterized.

**$[Ni_2L(o\text{-}O{-}C_6H_4{-}CHO)(H_2O)]\cdot 1.75H_2O$ ($\mathbf{4}\cdot 1.75H_2O$).** When a dilute methanol solution of $\mathbf{1}\cdot 3.25H_2O$ is left to slowly evaporate (four weeks), a small amount of crystals of $[Ni_2L(o\text{-}O{-}C_6H_4{-}CHO)(H_2O)]\cdot 1.75H_2O$, suitable for X-ray diffraction studies, was isolated.

**$[Ni_2L(OH)(H_2O)(MeOH)]\cdot 3H_2O$ ($\mathbf{5}\cdot 3H_2O$).** To a methanol (25 mL) solution of $\mathbf{1}\cdot 3.25H_2O$ (0.15 g, 0.11 mmol) in a previously dried Schlenk flask, $NMe_4OH\cdot 5H_2O$ (0.056 g, 0.31 mmol) was added under an argon (99.999%) stream. To the resultant solution, a methanol solution of $NMe_4OH\cdot 5H_2O$ (1 M) was added until a pH value of 12 (0.8 mL) was reached. Then, the solution was degasified and the flask filled with argon and stirred for 6 h. Concentration under a vacuum of the solution yielded green crystals of $[Ni_2L(OH)(H_2O)(MeOH)]\cdot 3H_2O\cdot 1.5MeOH$, suitable for X-ray diffraction studies. Crystals were filtered off using standard Schlenk techniques. Elemental analysis of the crystalline sample is in agreement with the stoichiometry $\mathbf{5}\cdot 3H_2O$, indicating that the crystals lose the most volatile solvent upon drying. Yield: 0.04 g (24.6%), mp > 300 °C. Anal. Calcd for $C_{28}H_{36}N_4Ni_2O_9$ (690.06): C, 48.74; H, 5.22; N, 8.12. Found: C, 48.95; H, 5.17; N, 8.29. MS($ES^+$): $m/z$ 571.2 ($[Ni_2L]^+$; 100%). IR (KBr, $\nu/cm^{-1}$): 1640 (C=N), 3390 ($OH_2$).

**$[Ni_2L(OAc)(MeOH)_2]\cdot H_2O\cdot 3MeOH$ ($\mathbf{6}\cdot H_2O\cdot 3MeOH$).** A methanol (15 mL) solution of $H_3L$ (0.3 g, 0.65 mmol) was added to a methanol (15 mL) solution of $Ni(OAc)_2\cdot 4H_2O$ (0.33 g, 1.31 mmol). To the resultant green solution were added $NMe_4OH\cdot 5H_2O$ (0.12 g, 0.65 mmol) and 10 mL of methanol. The mixture (pH = 7.0) was stirred in the air for 6 h, and the obtained green solution was left to slowly evaporate (five days) until green crystals of $[Ni_2L(OAc)(MeOH)_2]\cdot H_2O\cdot 3MeOH$, suitable for X-ray diffraction studies, were isolated. Crystals were filtered off and dried in the air. Yield: 0.31 g (58.9%), mp > 300 °C. Anal. Calcd for $C_{34}H_{52}N_4Ni_2O_{11}$ (810.22): C, 50.35; H, 6.41; N, 6.91. Found: C, 50.29; H, 6.26; N, 7.09. MS($ES^+$): $m/z$ 571.2 ($[Ni_2L]^+$, 100%). IR (KBr, $\nu/cm^{-1}$): 1641 (C=N), 3307 ($OH_2$).

Reaction of $\mathbf{6}\cdot H_2O\cdot 3MeOH$ with $NMe_4OH\cdot 5H_2O$ under an argon stream, following exactly the same method reported for the reaction of $\mathbf{1}\cdot 3.25H_2O$ in a basic medium under an inert atmosphere, yields, once more, $\mathbf{5}\cdot 3H_2O$, with 30.5% yield.

**$[\{Ni_2L(MeOH)\}(CO_3)\{Ni_2L(MeOH)_2\}]\cdot 4.75H_2O\cdot 2MeOH$ ($\mathbf{7}\cdot 4.75H_2O\cdot 2MeOH$).** To a methanol (25 mL) solution of $\mathbf{6}\cdot H_2O\cdot 3MeOH$ (0.15 g, 0.18 mmol) were added $NMe_4OH\cdot 5H_2O$ (0.1 g, 0.54 mmol) and 20 mL of methanol. The resultant green solution was basified with a methanol solution of $NMe_4OH\cdot 5H_2O$ (1 M) until a pH value of 12 was reached (0.8 mL). The mixture was stirred in the air for 6 h, and the obtained green solution was left to slowly evaporate (five days) until green crystals of $[\{Ni_2L(MeOH)\}(CO_3)\{Ni_2L(MeOH)_2\}]\cdot 4.75H_2O\cdot 2MeOH$, suitable for X-ray diffraction studies, were isolated. Crystals were filtered off and dried in the air. Yield: 0.0747 g (57.4%), mp > 300 °C. Anal. Calcd for $C_{60}H_{78}N_8Ni_4O_{18.75}$ (1446.14): C, 48.78; H, 5.61; N, 7.85. Found: C, 48.84; H, 5.41; N, 7.80. MS($ES^+$): $m/z$ 571.2 ($[Ni_2L]^+$, 100%). IR (KBr, $\nu/cm^{-1}$): 1640 (C=N), 3392 ($OH_2$).

**Crystallographic Measurements.** Crystal data and details of refinement are given in Table 1. Single crystals of $\mathbf{4}\cdot 1.75H_2O$ to $\mathbf{7}\cdot 4.75H_2O\cdot 2MeOH$, suitable for single-crystal X-ray studies, were obtained as detailed above. Diffraction data were collected for $\mathbf{4}\cdot 1.75H_2O$ (293 K), $\mathbf{5}\cdot 3H_2O\cdot 1.5MeOH$ (80 K), and $\mathbf{7}\cdot 4.75H_2O\cdot 2MeOH$ (100 K) using a BRUKER Smart-CCD-1000 diffractometer, employing graphite monochromated Mo-Kα radiation ($\lambda$ = 0.71073 Å). Data for $\mathbf{6}\cdot H_2O\cdot 3MeOH$ were recorded at 100 K on a FR591-Kappa CCD2000 Bruker-Nonius diffractometer, using monochromatic Cu-Kα radiation ($\lambda$ = 1.54178 Å) and a rotating anode generator. Data were corrected for Lorentz and polarization effects. Multiscan absorption corrections were applied using SADABS.[13]

The structures were solved by standard direct methods employing SHELXS-97[14] ($\mathbf{4}\cdot 1.75H_2O$, $\mathbf{6}\cdot H_2O\cdot 3MeOH$) or

(12) Fondo, M.; García-Deibe, A. M.; Ocampo, N.; Sanmartín, J.; Bermejo, M. R. *Dalton Trans.* **2007**, 414–416.

(13) (a) *SADABS*; Siemens Industrial Automation Inc.: Madison, WI, 1996. (b) Blessing, R. H. *Acta Crystallogr.* **1995**, *A51*, 33–38.

(14) Sheldrick, G. M. *SHELX97*; Institüt für Anorganische Chemie der Universität: Göttingen, Germany, 1998.

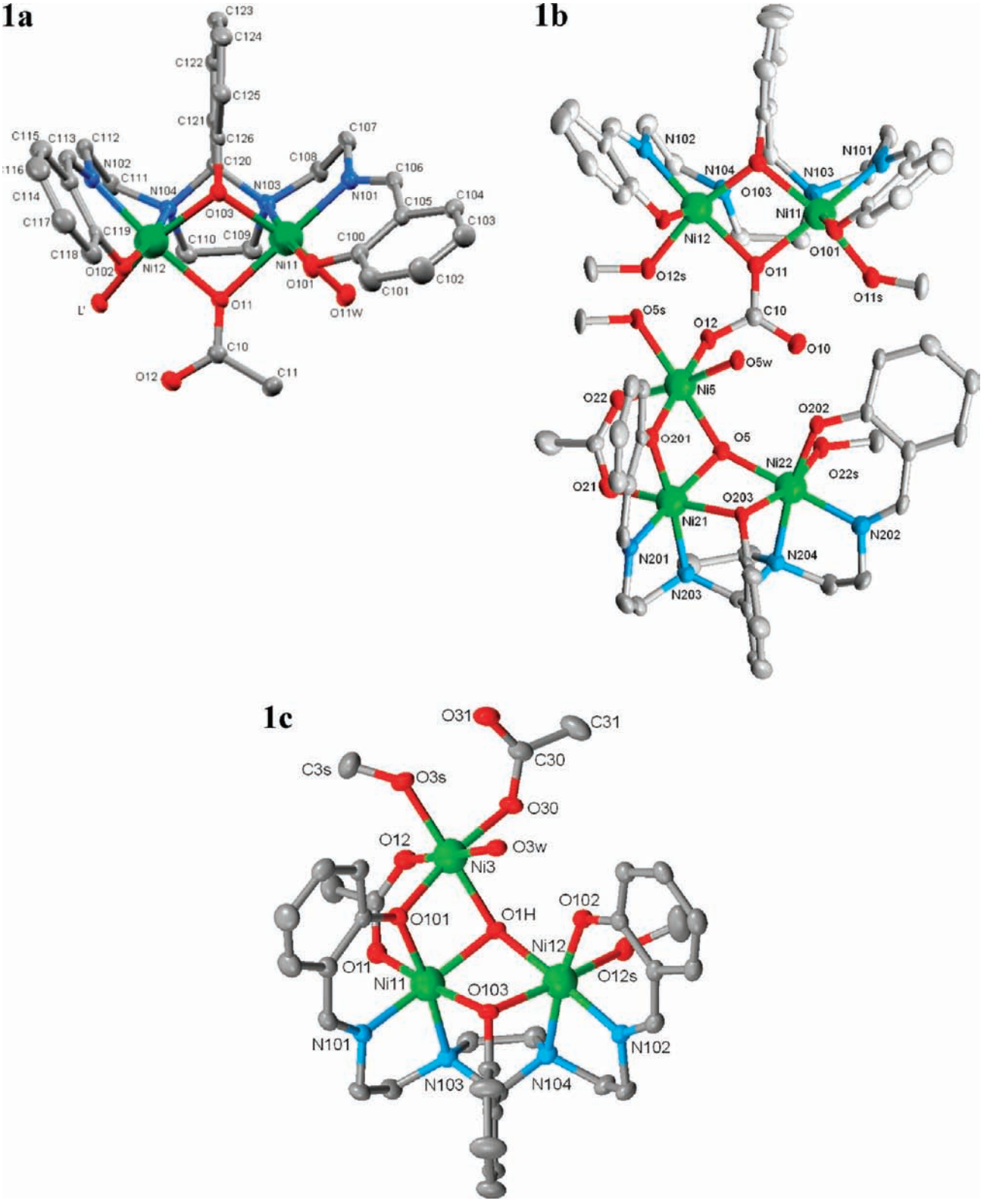


**Figure 1.** ORTEP diagram representing (1a) both cocrystallized dinuclear complexes in **1**, with L′ = $OH_2$ (**1a**) or L′ = $\eta^1$-$OHOCCH_3$ (**1b**); (1b) **2**; (1c) **3**.

SIR-92[15] (**5**·3$H_2O$·1.5MeOH, **7**·4.75$H_2O$·2MeOH) and refined by Fourier techniques based on $F^2$, using SHELXL-97.[14]

(15) SIR92 A program for crystal structure solution: Altomare, A.; Cascarano, G.; Giacovazzo, C.; Guagliardi, A. *J. Appl. Crystallogr.* **1993**, *26*, 343−350.

Non-hydrogen atoms were anisotropically refined. Hydrogen atoms were mostly included at geometrically calculated positions with thermal parameters derived from the parent atoms. Hydrogen atoms attached to water molecules or to groups suitable to form hydrogen bonds could be located on Fourier maps, fixed, and given isotropic displacement parameters of 0.08 Å$^2$ or ones depending on the parent atoms. Partial

**Table 1.** Crystal Data and Structure Refinement for **4**·1.75$H_2O$ to **7**·4.75$H_2O$·2MeOH

| | **4**·1.75$H_2O$ | **5**·3$H_2O$·1.5MeOH | **6**·$H_2O$·3MeOH | **7**·4.75$H_2O$·2MeOH |
|---|---|---|---|---|
| empirical formula | $C_{34}H_{37.5}N_4Ni_2O_{7.75}$ | $C_{29.5}H_{42}N_4Ni_2O_{10.5}$ | $C_{34}H_{52}N_4Ni_2O_{11}$ | $C_{60}H_{78}N_8Ni_4O_{18.75}$ |
| fw | 743.60 | 738.06 | 810.22 | 1446.14 |
| temp (K) | 293(2) | 80(2) | 100(2) | 100(2) |
| wavelength (Å) | 0.71073 | 0.71073 | 1.54178 | 0.71073 |
| cryst syst | monoclinic | triclinic | orthorhombic | monoclinic |
| space group | $P2_1/c$ | $P\bar{1}$ | $P2_12_12_1$ | $P2_1/c$ |
| $a$ (Å) | 11.5342(19) | 11.5932(16) | 13.804(1) | 18.567(6) |
| $b$ (Å) | 21.469(4) | 12.1572(17) | 14.843(1) | 15.566(5) |
| $c$ (Å) | 14.727(2) | 13.0326(18) | 18.306(1) | 24.071(7) |
| α (deg) | 90 | 106.232(2) | 90 | 90 |
| $\beta$ (deg) | 102.021(3) | 91.008(2) | 90 | 109.876(5) |
| $\gamma$ (deg) | 90 | 97.590(2) | 90 | 90 |
| $Z$ | 4 | 2 | 4 | 4 |
| abs coeff ($mm^{-1}$) | 1.108 | 1.137 | 1.435 | 1.210 |
| cryst size ($mm^3$) | 0.40 × 0.37 × 0.08 | 0.30 × 0.19 × 0.16 | 0.07 × 0.06 × 0.05 | 0.33 × 0.33 × 0.14 |
| reflns collected | 25384 | 17613 | 38129 | 95255 |
| independent reflns | 7234 [R(int) = 0.0342] | 6163 [$R_{int}$ = 0.0327] | 6854 [$R_{int}$ = 0.0787] | 11840 [$R_{int}$ = 0.0673] |
| data/restraints/params | 7234/0/432 | 6163/0/454 | 6854/0/485 | 11840/0/1097 |
| final $R$ indices [$I > 2\sigma(I)$] | $R_1$ = 0.0509 | $R_1$ = 0.0435 | $R_1$ = 0.0582 | $R_1$ = 0.0673 |
| | $wR_2$ = 0.1667 | $wR_2$ = 0.1160 | $wR_2$ = 0.1532 | $wR_2$ = 0.1435 |
| $R$ indices (all data) | $R_1$ = 0.1033 | $R_1$ = 0.0611 | $R_1$ = 0.0629 | $R_1$ = 0.1018 |
| | $wR_2$ = 0.1977 | $wR_2$ = 0.1244 | $wR_2$ = 0.1577 | $wR_2$ = 0.1483 |

occupancies of solvate molecules were individually refined and then rounded to simplify the formulas.

**Magnetic Measurements.** Magnetic susceptibility measurements for powder crystalline samples of **5**·3$H_2O$ to **7**·4.75$H_2O$·2MeOH were carried out at the Unitat de Mesures Magnètiques of the Universitat de Barcelona with a Quantum Design SQUID MPMS-XL susceptometer. The magnetic susceptibility data were recorded in the 2−300 K temperature range under magnetic fields of 400 G (2−30 K) and 7000 G (2−300 K). Diamagnetic corrections were estimated from Pascal's tables. The agreement factor is based on the function $R = \sum(\chi_M T_{exp} - \chi_M T_{cal})^2 / \sum(\chi_M T_{exp})^2$. Magnetic fields ranging from 0 to 50 000 G were used for magnetization measurements at 2 K.

**Computational Details.** The use of electronic structure calculations based on density functional theory provides an excellent estimation of the exchange coupling constants taking into account the tiny involved energy differences.[16,17] Since a detailed description of the computational strategy used to calculate the exchange coupling constants in polynuclear complexes is outside the scope of this paper, we will focus our discussion here to its most relevant aspects. Previously, we published a series of papers devoted to such a purpose, where more details can be found.[18−20] In the case of the $Ni_4$ tetranuclear complex (**7**), assuming no symmetry in the molecule, the spin Hamiltonian with six different $J$ values that we have employed is

$$\hat{H} = -2J_1\hat{S}_{11}\cdot\hat{S}_{12} - 2J_2\hat{S}_{21}\cdot\hat{S}_{22} - 2J_{3a}\hat{S}_{11}\cdot\hat{S}_{21} - 2J_{3b}\hat{S}_{12}\cdot\hat{S}_{22} - 2J_{4a}\hat{S}_{11}\cdot\hat{S}_{22} - 2J_{4b}\hat{S}_{12}\cdot\hat{S}_{21}$$

At a practical level, for the evaluation of the $n$ different coupling constants $J_{ij}$ present in a polynuclear complex, we need to carry out calculations for at least $n + 1$ different spin configurations. Thus, solving the system of $n$ equations obtained from the energy differences, we can obtain the $n$ coupling constants. In the case that more than $n$ spin distributions were calculated, a fitting procedure to obtain the coupling constants must be used. In the specific case of the studied $Ni_4$ complex, eight spin configurations have been employed to obtain the six indicated $J$ values: the high-spin solution ($S = 4$), the four $S = 2$ spin configurations corresponding to the inversion of one of the spins, and three $S = 0$ configurations obtained from the inversions of two spins {$Ni_{12}$, $Ni_{21}$}, {$Ni_{21}$, $Ni_{22}$}, and {$Ni_{12}$, $Ni_{22}$}.

All calculations were performed under the density functional theory approach, using the hybrid functional B3LYP[21] and the triple-ζ all-electron basis set for the nickel atoms, including two p polarization functions, while a double-ζ basis set was used for the other atoms.[22,23] The guess function was generated using the Jaguar 7.0 code.[24] Total energy calculations were performed using the Gaussian 03 code.[25]

The employed structural data in the calculation corresponds to that showing the higher occupancies (0.65), due to the disorder present for this complex structure. In our calculations, we have used the experimental structures that take into account small structural effects induced by intermolecular interactions, which may result in significant changes in the calculated exchange coupling constants, due to the strong dependence of the magnetic properties on structural parameters.

(16) Ruiz, E.; Alemany, P.; Alvarez, S.; Cano, J. *J. Am. Chem. Soc.* **1997**, *119*, 1297–1303.
(17) Ruiz, E.; Cauchy, T.; Cano, J.; Costa, R.; Tercero, J.; Alvarez, S. *J. Am. Chem. Soc.* **2008**, *130*, 7420–7426.
(18) Ruiz, E. *Struct. Bonding* (*Berlin*) **2004**, *113*, 71–102.
(19) Ruiz, E.; Rodríguez-Fortea, A.; Cano, J.; Alvarez, S.; Alemany, P. *J. Comput. Chem.* **2003**, *24*, 982–989.
(20) Ruiz, E.; Cano, J.; Alvarez, S.; Caneschi, A.; Gatteschi, D. *J. Am. Chem. Soc.* **2003**, *125*, 6791–6794.
(21) Becke, A. D. *J. Chem. Phys.* **1993**, *98*, 1372–1377.
(22) Schaefer, A.; Huber, C.; Ahlrichs, R. *J. Chem. Phys.* **1992**, *97*, 2571–2577.
(23) Schaefer, A.; Horn, C.; Ahlrichs, R. *J. Chem. Phys.* **1994**, *100*, 5829–5835.
(24) *Jaguar 7.0*; Schrödinger, Inc.: Portland, OR, 2007.
(25) Frisch, M. J.; Trucks, G. W.; Schlegel, H. B.; Scuseria, G. E.; Robb, M. A.; Cheeseman, J. R.; Montgomery, J. A.; Vreven, T.; Kudin, K. N.; Burant, J. C.; Millam, J. M.; Iyengar, S. S.; Tomasi, J.; Barone, V.; Mennucci, B.; Cossi, M.; Scalmani, G.; Rega, N.; Petersson, G. A.; Nakatsuji, H.; Hada, M.; Ehara, M.; Toyota, K.; Fukuda, R.; Hasegawa, J.; Ishida, H.; Nakajima, T.; Honda, Y.; Kitao, O.; Nakai, H.; Klene, M.; Li, X.; Knox, J. E.; Hratchian, H. P.; Cross, J. B.; Adamo, C.; Jaramillo, J.; Gomperts, R.; Stratmann, R. E.; Yazyev, O.; Austin, A. J.; Cammi, R.; Pomelli, C.; Ochterski, J.; Ayala, P. Y.; Morokuma, K.; Voth, G. A.; Salvador, P.; Dannenberg, J. J.; Zakrzewski, V. G.; Dapprich, S.; Daniels, A. D.; Strain, M. C.; Farkas, O.; Malick, D. K.; Rabuck, A. D.; Raghavachari, K.; Foresman, J. B.; Ortiz, J. V.; Cui, Q.; Baboul, A. G.; Clifford, S.; Cioslowski, J.; Stefanov, B. B.; Liu, G.; Liashenko, A.; Piskorz, P.; Komaromi, I.; Martin, R. L.; Fox, D. J.; Keith, T.; Al-Laham, M. A.; Peng, C. Y.; Nanayakkara, A.; Challacombe, M.; Gill, P. M. W.; Johnson, B.; Chen, W.; Wong, M. W.; Gonzalez, C.; Pople, J. A. *Gaussian 03*; Gaussian, Inc: Pittsburgh, PA, 2003.

**Scheme 1.** Reaction Scheme Studied for the $Ni(AcO)_2 \cdot 4H_2O/H_3L$ System

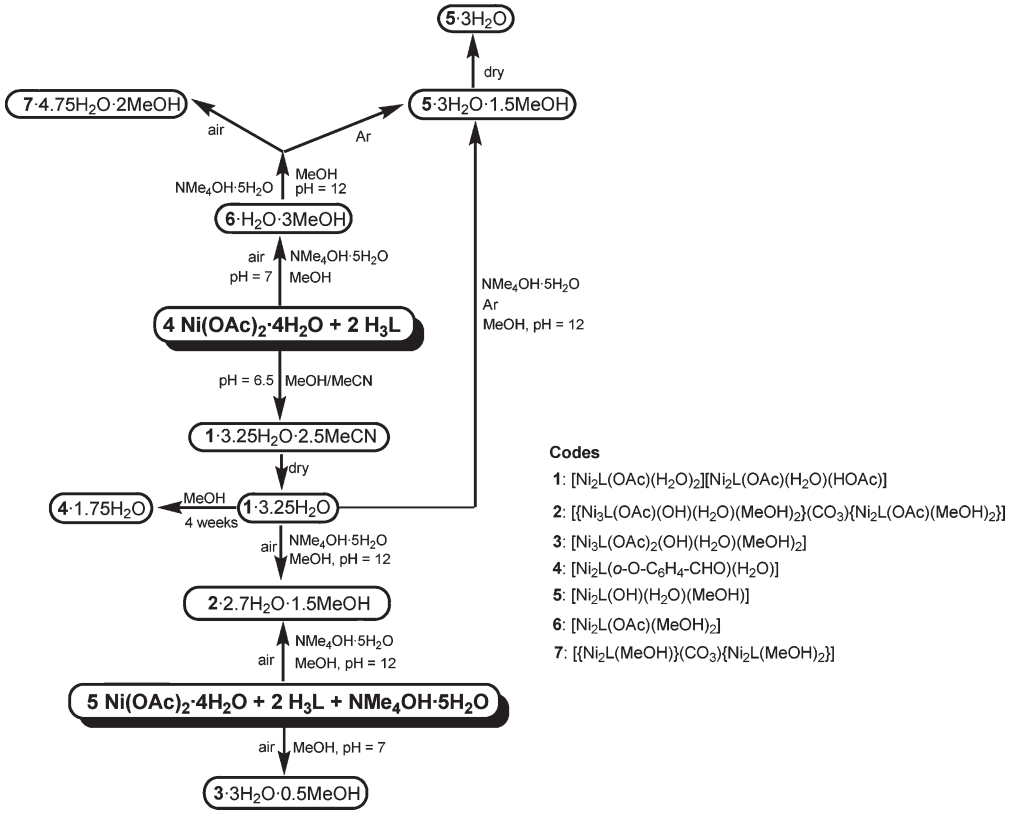


The use of the nonprojected energy of the broken symmetry solution as the energy of the low-spin state within the DFT framework provides good results because it avoids the cancellation of the nondynamic correlation effects, as stated in previous works.[19,26]

## Results and Discussion

**Synthesis.** In a previous communication,[12] we have reported that a mixture of $Ni(AcO)_2 \cdot 4H_2O$ with $H_3L$ in a 2:1 molar ratio generates a slightly acid solution (pH = 6.5), which upon concentration produced the double acetate complex $\mathbf{1} \cdot 3.25H_2O$ (Scheme 1, Figure 1a). Reaction of $\mathbf{1} \cdot 3.25H_2O$ in a strong basic alcoholic medium (pH = 12) in air gives rise to the pentanuclear complex $\mathbf{2} \cdot 2.7H_2O \cdot 1.5MeOH$ (Scheme 1, Figure 1b).

This unusual asymmetric $Ni_5$ cluster can also be obtained by spontaneous self-assembly, from a mixture of $Ni(AcO)_2 \cdot 4H_2O$ and $H_3L$ in a 5:2 molar ratio, in a basic methanol solution of pH = 12 (Scheme 1). However, when $Ni(AcO)_2 \cdot 4H_2O$, $H_3L$, and $NMe_4OH$ are mixed in 5:2:1 molar ratios, the concentration of the resultant solution of pH = 7 precipitates the trinuclear complex $\mathbf{3} \cdot 3H_2O \cdot 0.5MeOH$ (Scheme 1, Figure 1c), showing the profound influence of the pH of the medium on the nuclearity of the isolated complex.

Therefore, $\mathbf{2} \cdot 2.7H_2O \cdot 1.5MeOH$ can be prepared by two different routes, and a possible reaction mechanism for its obtainment from $\mathbf{1} \cdot 3.25H_2O$ was previously outlined[12] (Scheme 2). In the latter, we have postulated the presence of free Ni(II) ions in the reaction medium, joined to the formation of a hydroxide intermediary. Now, both suppositions appear to be corroborated (Scheme 1). Thus, when a methanol solution of $\mathbf{1} \cdot 3.25H_2O$ is left to stand for 4 weeks, it undergoes partial hydrolysis to yield $\mathbf{4} \cdot 1.75H_2O$ as a byproduct. This process should be reasonably accompanied by a release of Ni(II) ions in the reaction medium. Moreover, $\mathbf{1} \cdot 3.25H_2O$ reacts under an argon atmosphere in a strong basic medium (pH = 12) to generate the hydroxide complex $\mathbf{5} \cdot 3H_2O \cdot 1.5MeOH$. Consequently, the identification of both $\mathbf{4} \cdot 1.75H_2O$ and $\mathbf{5} \cdot 3H_2O \cdot 1.5MeOH$ further supports the proposed reaction mechanism.

In addition, since $\mathbf{1} \cdot 3.25H_2O$ contains an acetic acid ligand, it was thought that the neutralization of the acetic acid should produce a symmetric acetate complex, as it is. Accordingly, when nickel(II) acetate, $H_3L$, and $NMe_4OH \cdot 5H_2O$ are mixed in 2:1:1 molar ratios in the air, a mixture of pH = 7 is obtained, which upon concentration precipitates $\mathbf{6} \cdot H_2O \cdot 3MeOH$ (Scheme 1). The reactivity of this new acetate compound in a basic medium was investigated both in the air and under an argon stream, showing that the atmosphere plays a fundamental role in the reaction pattern. Thus, the reaction of $\mathbf{6} \cdot H_2O \cdot 3MeOH$ with $NMe_4OH \cdot 5H_2O$ (pH = 12) under argon gives rise to the hydroxide complex $\mathbf{5} \cdot 3H_2O \cdot 1.5MeOH$, which, as mentioned, can also be isolated from $\mathbf{1} \cdot 3.25H_2O$. In contrast, the same reaction in the air produces the tetranuclear complex $\mathbf{7} \cdot 4.75H_2O \cdot 2MeOH$. This compound contains a carbonate ligand, which seems to come from atmospheric carbon dioxide fixation. Bearing in mind that the hydroxide complex **5** could be isolated in an inert atmosphere, a possible mechanism for the assemblage of **7** from **6** can be rationalized according to that shown in Scheme 3.

(26) Ruiz, E.; Alvarez, S.; Cano, J.; Polo, V. *J. Chem. Phys.* **2005**, *123*, 164110/1–164110/7.

**Scheme 2.** Reaction Mechanism Proposed for the Isolation of **2** from **1**[12 a]

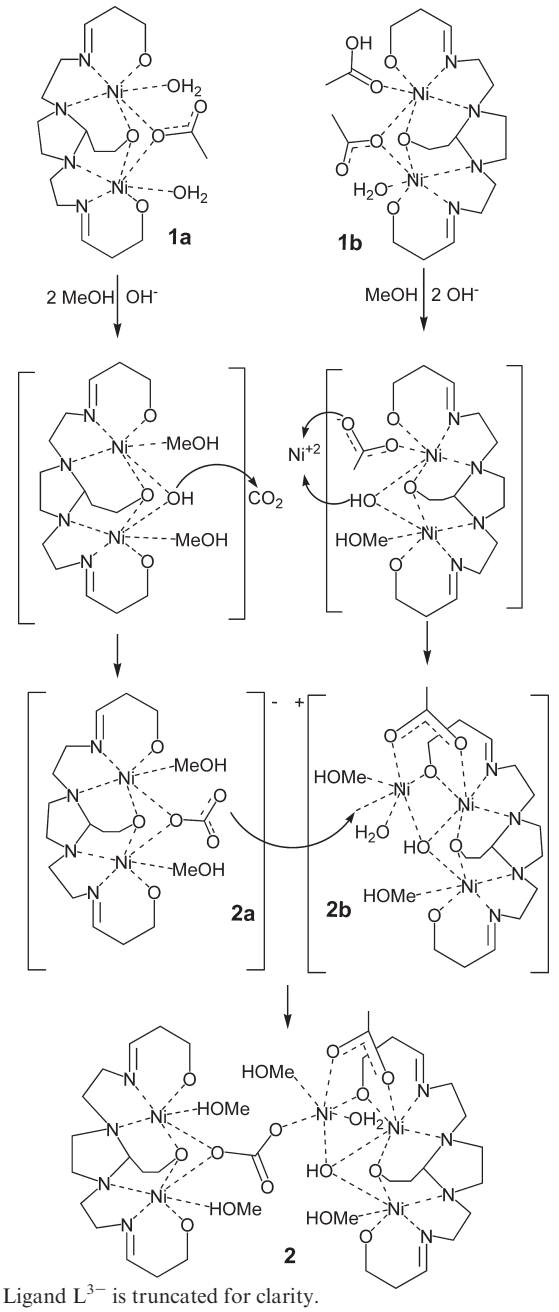


[a] Ligand $L^{3-}$ is truncated for clarity.

As a result, all of the performed experiments, which are summarized in Scheme 1, show that the nuclearity of nickel(II) complexes containing $L^{3-}$ critically depends not only on the stoichiometry of the reaction but also on the pH, and on the atmosphere of the medium.

Complexes **5** to **7** were fully characterized by elemental analysis, IR spectroscopy, electrospray mass spectrometry, X-ray diffraction studies, and magnetic measurements. Complex **4**·1.75$H_2O$ was isolated as a byproduct, as previously stated, and consequently, it was only crystallographically characterized.

The elemental analyses were recorded on dried crystals and agree with the formulations **5**·3$H_2O$, **6**·$H_2O$·3MeOH, and **7**·4.75$H_2O$·2MeOH, showing that **5**·3$H_2O$·1.5MeOH loses the most volatile solvent upon drying. The IR spectra of the complexes show a strong band at about 1640 $cm^{-1}$, assigned to $\nu(CN_{imine})$, in accordance with the coordination of the ligand to the metal ions through the imine nitrogen atoms. In addition, a broad band centered between 3300 and 3400 $cm^{-1}$ agrees with the hydration of the compounds. The mass spectra of all of the complexes show a peak of 100% intensity at ca. 571 $m/z$, assignable to the fragment $[Ni_2L]^+$. No peaks of higher mass were observed for any of the compounds, maybe due to their neutral nature.

**Description of the Crystal Structures.** Single crystals of **4**·1.75$H_2O$, **5**·3$H_2O$, **6**·$H_2O$·3MeOH, and **7**·4.75$H_2O$·2MeOH, suitable for X-ray structure determination, were obtained as detailed above.

**4·1.75$H_2O$, 5·3$H_2O$·1.5MeOH, and 6·$H_2O$·3MeOH.** The three complexes are quite similar, so they will be discussed together. ORTEP views of them are shown in Figures 2, 3 and 4. Experimental details are given in Table 1, and main distances and angles are listed in Tables 2 and 3.

The crystal structures of **4**·1.75$H_2O$ to **6**·$H_2O$·3MeOH show that they consist of binuclear $[Ni_2L(X)(MeOH)(Y)]$ units (X = *o*-O-$C_6H_4$-CHO, Y = $H_2O$ for **4**; X = OH, Y = $H_2O$ for **5**; and X = OAc, Y = MeOH for **6**), with different solvates. In all of these complexes, the heptadentate Schiff base $L^{3-}$ accommodates two nickel ions in its two $N_2O$ compartments. Each one of them is formed by contiguous imine (N101 or N102) and imidazolidine nitrogen atoms (N103 or N104) and a terminal phenol O atom (O101 or O102), with the imidazolidine NCN group (N103C120N104) spanning both nickel ions. In addition, the central phenol oxygen atom (O103) bridges both metal atoms. Thus, as usual,[1−8] the Schiff base provides $N_2O_2$ environments around the nickel centers. The main difference among the three complexes arises from the filling of the coordination spheres by exogenous donors: a $\mu$-$\eta^1$:$\eta^1$-O,O salicylaldehydate anion and a water ligand in **4** (Figure 2); a hydroxide bridge, a water, and a methanol molecule in **5** (Figure 3); and a monodentate acetate bridge and two methanol molecules in **6** (Figure 4). Hence, all of the nickel ions are $N_2O_4$-hexacoordinated and triply bridged by the *NCN* group and two oxygen atoms, one endogenous and the other one exogenous.

This leads to intramolecular Ni11···Ni12 separations of ca. 3.1 Å, and Ni−O−Ni angles ranging from 95.4 to 98.4°, the distances and angles about the metal centers being in agreement with distorted octahedral environments.

The described features show that the symmetry of **4** and **5** is reduced respect of that of **6**, so that complexes **4** and **5** possess stereoisomery, with both enantiomers present in the unit cell (50%). Unpredictably, in spite of a theoretical $C_s$ symmetry for **6**·$H_2O$·3MeOH, it crystallizes in the chiral $P2_12_12_1$ space group of the orthorhombic system, with absolute structure Flack parameter[27] of 0.002(38), and, therefore, not only the **6**·$H_2O$·3MeOH molecules are chiral, but the supramolecular architecture is chiral as well. This feature appears astonishing, since the coordination environments and ligands (endogenous and exogenous) show a total symmetry in **6**.

The asymmetry of **6** in this crystal structure actually results from the heading of the uncoordinated acetate

(27) Flack, H. D. *Acta Crystallogr.* **1983**, *A39*, 876–881.

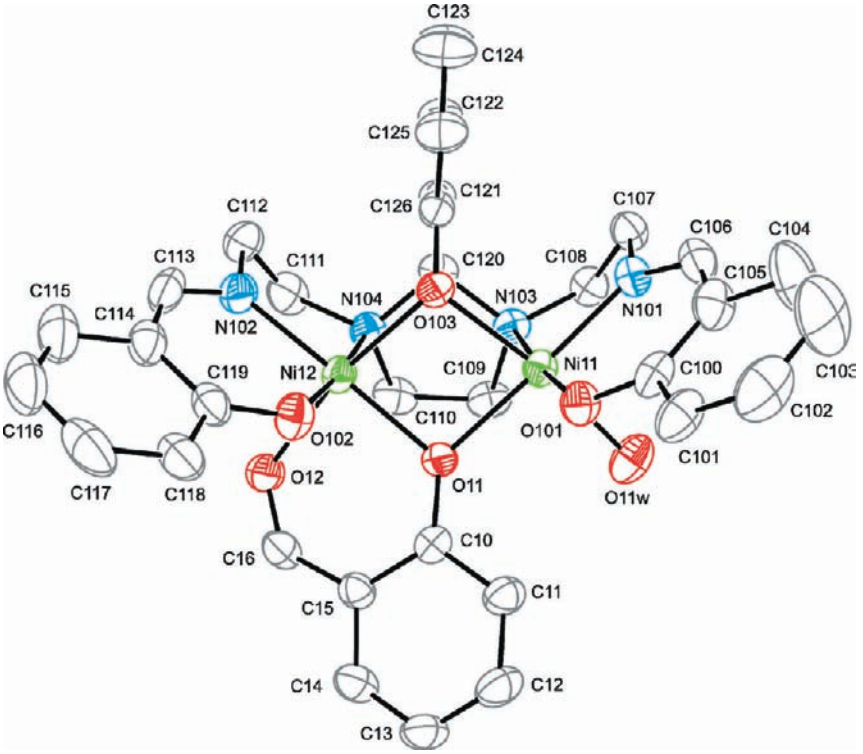


**Figure 2.** An ORTEP view of the crystal structure of **4**. Hydrogen atoms are omitted for clarity. Thermal ellipsoids are shown at the 40% probability level.

**Scheme 3.** A Possible Reaction Pathway for the Obtaining of **7** from **6**[a]

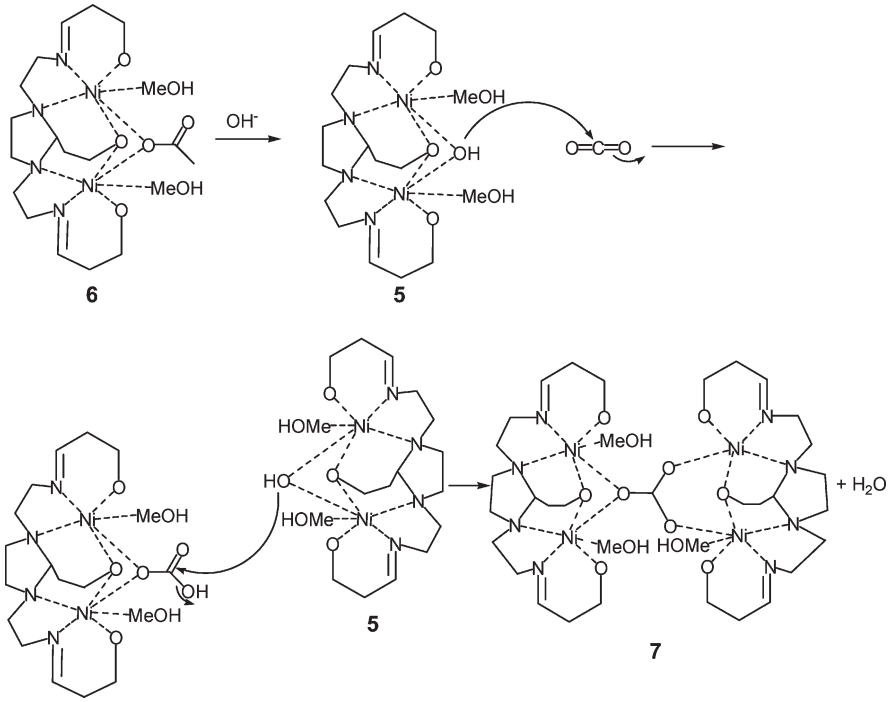


[a] Ligand $L^{3-}$ is truncated for clarity.

O atom toward only one of the methanol ligands, because of a classic intramolecular hydrogen bond. For that reason, this complex presents conformational isomery, but not stereoisomery and, of course, only in the solid state. In this way, the studied crystal only contains one of the conformers in the unit cell. This can be understood as that complex molecule where the uncoordinated O atom of the bridging acetate group points to the coordinated methanol molecule placed on the left, when we consider that the imidazolidine ring is behind the Ni···Ni axis, and the central arm is pointing up, such as Figure 4 illustrates.

Regarding the homochirality of the crystal structure of $\mathbf{6}\cdot H_2O\cdot 3MeOH$, it is the result of spontaneous resolution during crystallization, and it is also based on the hydrogen bond scheme but, in this case, is intermolecular.

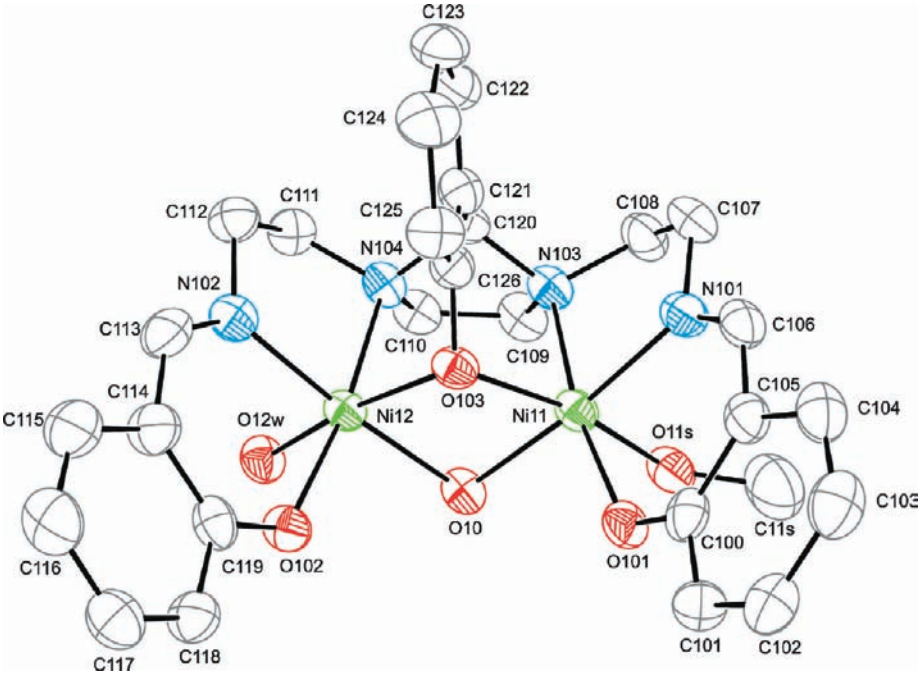


**Figure 3.** An ORTEP view of the crystal structure of **5**. Hydrogen atoms are omitted for clarity. Thermal ellipsoids are shown at the 40% probability level.

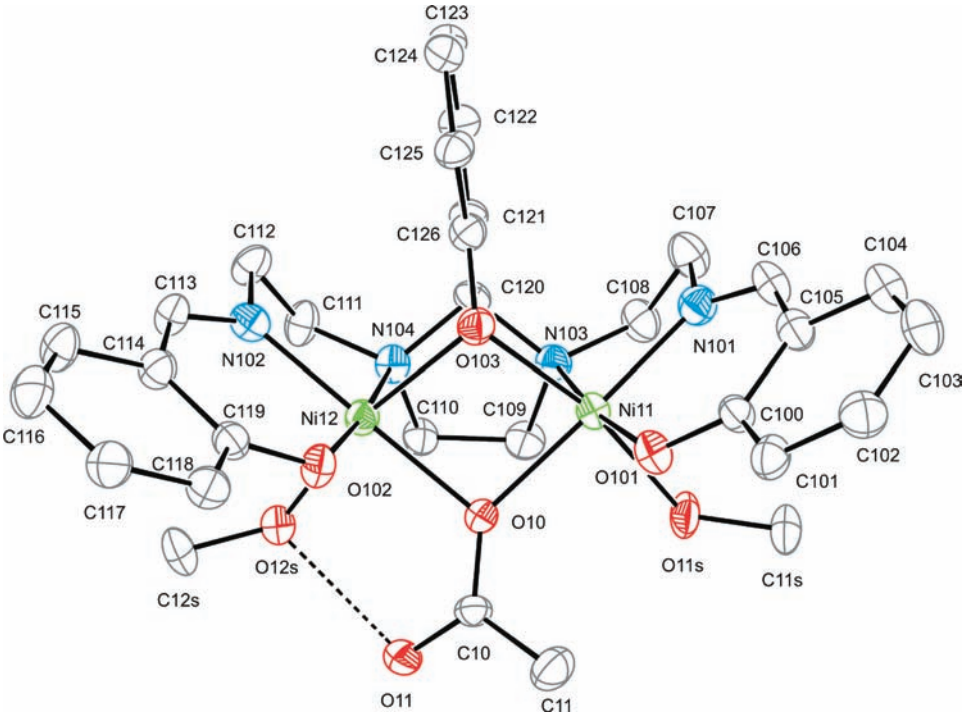


**Figure 4.** An ORTEP view of the crystal structure of **6**. Hydrogen atoms are omitted for clarity. Thermal ellipsoids are shown at the 40% probability level.

This leads to the formation of helical chains, which are parallel to *c* and result from the interactions among this conformer, the water, and the methanol solvates. All of these chains display a Δ configuration (Figure 5).

The fact that the chirality of $\mathbf{6}\cdot H_2O\cdot 3MeOH$ is based on hydrogen bonds is, as far as we know, a quite uncommon feature, but it is even more exceptional that this kind of interaction is the base of the homochirality of the crystalline structure, totally constructed from achiral molecules.[28] This situation is a bit more frequent when we consider chiral molecules per se.[29]

(28) Prins, L. J.; Jong, F. De; Timmerman, P.; Reinhoudt, D. N. *Nature* **2000**, *408*, 181–184.

(29) (a) Matsumoto, K.; Ozawa, T.; Jitsukawa, K.; Einaga, H.; Masuda, H. *Chem. Commun* **2001**, 978–979. (b) Hirschberg, J. H. K. K.; Koevoets, R. A.; Sijbesma, R. P.; Meijer, E. W. *Chem.—Eur. J.* **2003**, *9*, 4222–4231. (c) Takahashi, S.; Katagiri, T.; Uneyama, K. *Chem. Commun*. **2005**, 3658–3660. (d) Enamullah, M.; Sharmin, A.; Hasegawa, M.; Hoshi, T.; Chamayou, A.-C.; Janiak, C. *Eur. J. Inorg. Chem*. **2006**, 2146–2154. (e) Brewer, C. T.; Brewer, G.; Butcher, R. J.; Carpenter, E. E.; Schiemiedekamp, A. M.; Viragh, C. *Dalton Trans*. **2007**, 295–298.

**Table 2.** Main Bond Distances (Å) and Angles (deg) for **4**·1.75$H_2O$

| | | | |
|---|---|---|---|
| Ni11−N101 | 2.003(4) | N101−Ni11−O11 | 175.83(16) |
| Ni11−N103 | 2.177(4) | O103−Ni11−O11W | 171.76(15) |
| Ni11−O101 | 1.985(3) | O101−Ni11−N103 | 174.17(15) |
| Ni11−O103 | 2.085(3) | N102−Ni12−O1X | 176.96(17) |
| Ni11−O11 | 2.079(3) | O103−Ni12−O12 | 168.62(15) |
| Ni11−O11W | 2.178(4) | O102−Ni12−N104 | 173.16(15) |
| Ni12−N102 | 1.996(5) | Ni11−O103−Ni12 | 95.40(14) |
| Ni12−N104 | 2.187(4) | Ni11−O1X−Ni12 | 97.44(15) |
| Ni12−O102 | 2.017(4) | | |
| Ni12−O103 | 2.074(3) | | |
| Ni12−O11 | 2.013(3) | | |
| Ni12−O12 | 2.110(4) | | |
| Ni11···Ni12 | 3.0753(11) | | |

**Table 3.** Main Bond Distances (Å) and Angles (deg) for **5**·$H_2O$·3MeOH and **6**·3$H_2O$·1.5MeOH

| | **5**·3$H_2O$·1.5MeOH | **6**·$H_2O$·3MeOH |
|---|---|---|
| Ni11−N101 | 2.019(3) | 2.023(4) |
| Ni11−N103 | 2.167(3) | 2.179(4) |
| Ni11−O101 | 2.051(3) | 2.010(3) |
| Ni11−O103 | 2.043(2) | 2.066(3) |
| Ni11−O10 | 2.082(3) | 2.079(3) |
| Ni11−O11S | 2.102(3) | 2.165(3) |
| Ni12−N102 | 2.009(3) | 1.993(4) |
| Ni12−N104 | 2.173(3) | 2.176(4) |
| Ni12−O102 | 2.043(3) | 2.010(3) |
| Ni12−O103 | 2.057(3) | 2.078(3) |
| Ni12−O10 | 2.065(3) | 2.096(3) |
| Ni12−O12X[a] | 2.112(3) | 2.141(3) |
| Ni11···Ni12 | 3.0934(8) | 3.1357(11) |
| N101−Ni11−O10 | 173.80(12) | 175.38(14) |
| O103−Ni11−O11S | 168.00(11) | 166.96(13) |
| O101−Ni11−N103 | 170.95(11) | 171.87(13) |
| N102−Ni12−O10 | 174.83(12) | 178.69(14) |
| O103−Ni12−O12X[a] | 169.47(11) | 166.13(12) |
| O102−Ni12−N104 | 172.52(11) | 174.72(14) |
| Ni11−O103−Ni12 | 97.94(10) | 98.34(12) |
| Ni11−O10−Ni12 | 96.49(11) | 97.37(12) |

[a] X = W for **5** and S for **6**.

In the case of **4**·1.75$H_2O$ and **5**·3$H_2O$·1.5MeOH, the molecules of solvate also participate in hydrogen bond interactions with the metal complexes, but these interactions lead to different assemblies. Accordingly, in **4**·1.75$H_2O$, a trifurcated hydrogen bond between a water solvate, the water ligand of one complex, and the external phenol oxygen donors of a second complex also expand the binuclear units into chains.

In **5**·3$H_2O$·1.5MeOH, several hydrogen bonds involving water solvates and coordinated water, methanol, and hydroxide ligands, as well as the external phenol oxygen atoms of the Schiff base, keep two molecules of the complex in close proximity, resembling a tetranuclear cluster by the interaction of two binuclear units (Figure 6). These pseudotetranuclear associations are connected via long-order hydrogen-bond interactions, expanding the pseudotetranuclear rectangles, with sides of ca. 3.09 and 4.83 Å, in a 3D network.

**7·4.75$H_2O$·2MeOH.** An ORTEP view of **7**·4.75$H_2O$·2MeOH is represented in Figure 7. Experimental details are summarized in Table 1, and main distances and angles are reported in Table 4.

This crystal structure shows that the unit cell of **7**·4.75$H_2O$·2MeOH is composed of [{$Ni_2$L(MeOH)}-($CO_3$){$Ni_2$L(MeOH)$_2$}] molecules, in addition to water and methanol as solvates. Therefore, **7** is a neutral tetranuclear complex that can be understood as being made up from two slightly different binuclear units, $[Ni_2L(MeOH)]^+$ (**7a**) and $[Ni_2L(MeOH)_2)]^+$ (**7b**), which are joined by a carbonate ligand. It should be mentioned that almost the whole Schiff base, as well as the methanol ligands, and even the nickel atoms of **7b**, are disordered over two sites, with occupancies of 0.65 and 0.35, respectively. The ORTEP diagram shown in Figure 7 represents the positions with higher occupancies.

In both **7a** and **7b**, the Schiff base ligand acts as in **4** to **6**, providing a $N_2O_2$ environment around each nickel ion. The coordinated methanol molecules make the main difference between both binuclear cations: in **7b**, each nickel ion is coordinated to a methanol ligand, while in **7a**, just a methanol molecule coordinates to a nickel atom (Ni11). The coordination spheres of both binuclear cationic moieties are completed by an exogenous carbonate ligand, acting as a $\mu_4$ donor: two of its oxygen atoms (O11 and O12) bridge both nickel atoms of the **7a** cation in a $\mu_2$-$\eta^1$:$\eta^1$ fashion, whereas O10 behaves as a $\mu_2$ bridge between the nickel ions of the **7b** unit. Accordingly, the metal centers of **7b** are hexacoordinated, as it is Ni11 of **7a**, while Ni12 (**7a**) is pentacoordinated in a $N_2O_3$ environment. Thus, the metal atoms present two different geometries: distorted octahedral for Ni11, Ni21, and Ni22 and slightly distorted square-pyramidal for Ni12 ($\tau$ parameter[30] of 0.049), with the carbonate oxygen atom O12 occupying the apical site of the pyramid. It should be noted that this latter geometry is highly unusual for nickel complexes with this kind of ligand, which invariably shows an octahedral environment.[3c,5d,6d,7c,12] In addition, the asymmetry shown by the complex leads to chirality, but once more, both enantiomers are present in the unit cell at 50%.

In this case, the structure of **7** can be described as a molecular rectangle, with distances between the nickel ions that reflect the different numbers and natures of the bridges. Hence, (a) the Ni11···Ni12 and Ni21···Ni22 pairs are triple-bridged ($NCN_{imidazolidine}$, endogenous phenol oxygen atom, and O or $OCO_{carbonato}$), with Ni···Ni distances of ca. 3 Å, and (b) the Ni11···Ni21 and Ni12···Ni22 pairs are single-bridged by the carbonato ligand, in a syn−anti $\mu$-$\eta^1$:$\eta^1$-O,O′ mode, with longer Ni···Ni distances, of ca. 5 Å.

Finally, it is worth noting that the coordination mode shown by the carbonate ligand, as far as we know, has not been previously reported for nickel complexes, although it has been found in some copper,[6c,31−33] cobalt,[34] or zinc[6a,b,35,36] compounds.

**Magnetic Studies.** The magnetic properties of **5**·3$H_2O$, **6**·$H_2O$·MeOH, and **7**·4.75$H_2O$·2MeOH have been investigated in the 2−300 K temperature range.

(30) Addison, A. W.; Rao, T. N.; Reedijk, J.; Van Rijk, J.; Verschoor, G. C. *J. Chem. Soc., Dalton Trans.* **1984**, 1349–1356.
(31) Einstein, F. W. B.; Willis, A. C. *Inorg. Chem.* **1981**, *20*, 609–614.
(32) Escuer, A.; Peñalba, E.; Vicente, R.; Solans, X.; Font-Badía, M. J. *J. Chem. Soc., Dalton Trans.* **1997**, 2315–2319.
(33) Rodríguez, M.; Llobet, A.; Corbella, M.; Müller, P.; Usón, M. A.; Martell, A. E.; Reibenspens, J. *J. Chem. Soc., Dalton Trans.* **2002**, 2900–2906.
(34) Armentano, D.; De Munno, G.; Lloret, F.; Julve, M. *Inorg. Chem.* **1999**, *38*, 3744–3747.
(35) Döring, M.; Ciesielski, M.; Walter, O.; Görls, H. *Eur. J. Inorg. Chem.* **2002**, 1615–1621.
(36) Bauer-Siebenlist, B.; Meyer, F.; Vidovic, D.; Pritzkow, H. *Z. Anorg. Allg. Chem.* **2003**, *629*, 2152–2156.

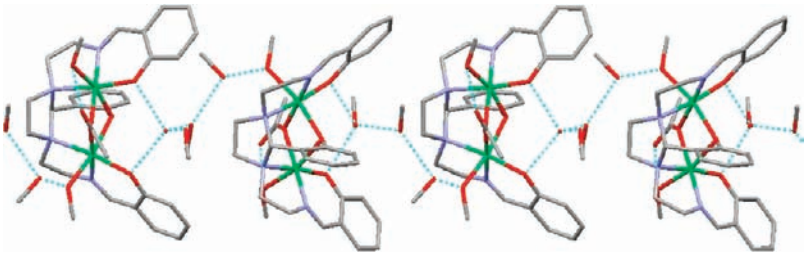

**Figure 5.** A view (omitting H atoms for clarity) of a fragment of the H-bonded helical array of $6 \cdot H_2O \cdot 3MeOH$, showing the Δ configuration.

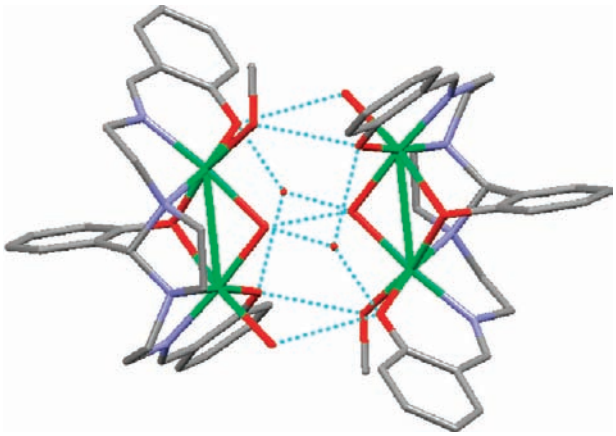

**Figure 6.** A view (omitting H atoms for clarity) of the H-bond scheme between two molecules (enantiomers) of **5**, resembling a tetranuclear molecular rectangle.

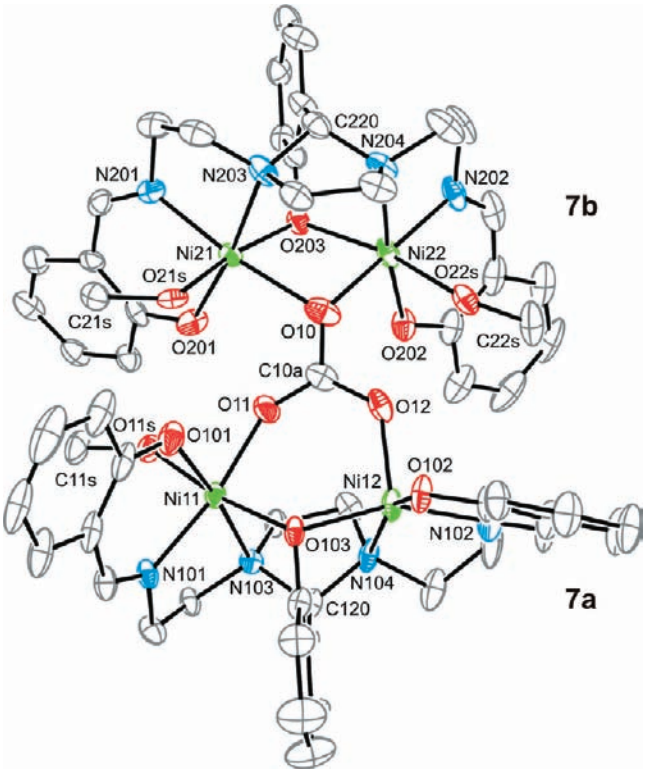


**Figure 7.** An ORTEP view of the crystal structure of **7**. Hydrogen atoms and carbon labels, except those corresponding to bridges, are omitted for clarity. Thermal ellipsoids are shown at the 40% probability level.

$5 \cdot 3H_2O$ and $6 \cdot H_2O \cdot MeOH$ are binuclear complexes with similar magnetic behavior. Plots of $\chi_M T$ versus $T$ for $5 \cdot 3H_2O$ and $6 \cdot H_2O \cdot MeOH$ are shown in Figure 8 and Figure S1 (Supporting Information), respectively. In both cases, the $\chi_M T$ value at 300 K (2.58 $cm^3\ mol^{-1}\ K$ for $5 \cdot 3H_2O$ and 2.97 $cm^3\ mol^{-1}\ K$ for $6 \cdot H_2O \cdot MeOH$) is higher than the expected one for two uncoupled Ni(II) ions with $g = 2$ (2.0 $cm^3\ mol^{-1}\ K$), and this value increases upon cooling to reach a maximum at low temperatures. Then, the product decreases with decreasing temperature for both complexes. Thus, the observed behavior indicates an intramolecular ferromagnetic interaction between Ni(II) ions, with the decreasing in $\chi_M T$ at low temperatures being attributed to either interbinuclear antiferromagnetic interactions or the effect of the zero field splitting of the ground state. The intramolecular ferromagnetic coupling is also corroborated by magnetization measurements at 2 K. In both cases, the $M/N\beta$ versus $H$ curves tend to 4 at 5 T, suggesting an $S = 2$ ground state.

Susceptibility curves were treated with the MAGPACK program,[37] where the exchange spin Hamiltonian is expressed as $H = -2\sum J_{ij}S_iS_j$. The best fit of the curves with this program, including the $D_{Ni}$ and $zJ'$ parameters, give the values $2J = 8.0\ cm^{-1}$, $g = 2.21$, $|D_{Ni}| = 5.59\ cm^{-1}$, $zJ' = -0.63\ cm^{-1}$, and TIP $= 3.0 \times 10^{-4}\ cm^3\ mol^{-1}$ ($R = 7.19 \times 10^{-6}$) for $5 \cdot 3H_2O$ and $2J = 5.1\ cm^{-1}$, $g = 2.38$, $|D_{Ni}| = 5.50\ cm^{-1}$, $zJ' = -0.39\ cm^{-1}$, and TIP $= 3.0 \times 10^{-4}\ cm^3\ mol^{-1}$ ($R = 1.43 \times 10^{-4}$) for $6 \cdot H_2O \cdot 3MeOH$.

The $2J$ values are completely consistent with reported results for binuclear complexes with a $Ni_2O_2$ core bearing an additional NCN bridge,[3c,5d,6d,7c] and the $|D_{Ni}|$ parameter is in the range of the expected one for a nickel(II) ion in a distorted octahedral environment.[38] It should be noted that it was not possible to obtain a good fit of the $\chi_M T$ versus $T$ experimental graph excluding the $zJ'$ term, which is in agreement with the extended hydrogen bond scheme observed in the crystal structures.

A plot of $\chi_M T$ versus $T$ for $7 \cdot 4.75H_2O \cdot 2MeOH$ is shown in Figure 9. In this case, the $\chi_M T$ product at 300 K is 5.50 $cm^3\ mol^{-1}\ K$, and this value continuously diminishes with decreasing temperature. Therefore, an overall intramolecular antiferromagnetic coupling is operative in this compound. Magnetization measurements at 2 K show an almost linear variation of $M/N\beta$ versus $T$, which tends to 2.5 at 5 T without reaching saturation, corroborating the global antiferromagnetic behavior.

(37) (a) Borrás-Almenar, J. J.; Clemente, J. M.; Coronado, E.; Tsukerblat, B. S. *Inorg. Chem.* **1999**, *38*, 6081–6088. (b) Borrás-Almenar, J. J.; Clemente, J. M.; Coronado, E.; Tsukerblat, B. S. *J. Comput. Chem.* **2001**, *22*, 985–991.

(38) Boca, R. *Coord. Chem. Rev.* **2004**, *248*, 757–815.

**Table 4.** Main Bond Distances (Å) and Angles (deg) for $7\cdot4.75H_2O\cdot2MeOH$[a]

| | | | |
|---|---|---|---|
| Ni11−O11 | 1.984(4) | | |
| Ni11−N101 | 2.002(4) | | |
| Ni11−O101 | 2.016(4) | | |
| Ni11−O103 | 2.026(3) | | |
| Ni11−O11S | 2.151(4) | | |
| Ni11−N103 | 2.156(4) | | |
| Ni12−O102 | 1.956(4) | | |
| Ni12−O12 | 1.972(5) | | |
| Ni12−N102 | 1.979(5) | | |
| Ni12−O103 | 2.009(3) | | |
| Ni12−N104 | 2.174(4) | | |
| Ni21−O201 | 2.002(5) | Ni1′−O201 | 2.141(7) |
| Ni21−N201 | 2.029(8) | Ni1′−N21 | 2.005(16) |
| Ni21−O203 | 2.048(8) | Ni1′−O23 | 2.030(15) |
| Ni21−O10 | 2.157(5) | Ni1′−O10 | 1.841(7) |
| Ni21−O21S | 2.166(19) | Ni1′−O1S′ | 2.101(18) |
| Ni21−N203 | 2.186(15) | Ni1′−N23 | 2.18(3) |
| Ni22−O10 | 1.969(5) | Ni2′−O10 | 2.243(7) |
| Ni22−O202 | 1.994(9) | Ni2′−O22 | 2.006(18) |
| Ni22−N202 | 2.007(10) | Ni2′−N22 | 1.99(2) |
| Ni22−O203 | 2.079(8) | Ni2′−O23 | 2.047(14) |
| Ni22−N204 | 2.159(11) | Ni2′−N24 | 2.14(2) |
| Ni22−O22S | 2.170(10) | Ni2′−O2S′ | 2.150(19) |
| Ni11···Ni12 | 3.4126(15) | | |
| Ni21···Ni22 | 3.123(4) | Ni1′···Ni2′ | 3.114(7) |
| Ni11···Ni21 | 4.773(3) | | |
| Ni12···Ni22 | 5.300(4) | | |
| O11−Ni11−N101 | 169.83(17) | | |
| O103−Ni11−O11S | 169.77(17) | | |
| O101−Ni11−N103 | 173.57(17) | | |
| N102−Ni12−O103 | 155.92(18) | | |
| O102−Ni12−N104 | 158.94(17) | | |
| Ni11−O103−Ni12 | 115.51(17) | | |
| N201−Ni21−O10 | 171.7(3) | N21−Ni1′−O10 | 169.9(6) |
| O203−Ni21−O21S | 169.3(3) | O23−Ni1′−O1S′ | 172.7(8) |
| O201−Ni21−N203 | 172.9(4) | O201−Ni1′−N23 | 163.7(6) |
| O10−Ni22−N202 | 177.1(3) | O10−Ni2′−N22 | 172.8(7) |
| O202−Ni22−N204 | 172.9(4) | O22−Ni2′−N24 | 174.5(7) |
| O203−Ni22−O22S | 164.5(3) | O23−Ni2′−O2S′ | 163.9(8) |
| Ni21−O203−Ni22 | 98.3(3) | Ni1′−O23−Ni2′ | 99.7(7) |
| Ni22−O10−Ni21 | 98.28(19) | Ni1′−O10−Ni2′ | 98.9(3) |

[a] The ′ corresponds to the location of lower occupancy (35%) of the disordered atoms.

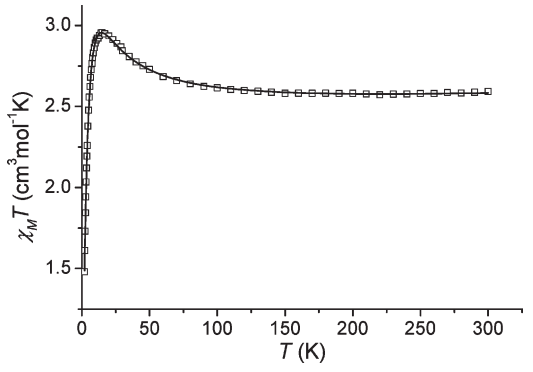


**Figure 8.** Plot of $\chi_M T$ versus $T$ for $5\cdot3H_2O$. (□) Experimental data, (—) best fit (see text).

The structural analysis for $7\cdot4.75H_2O\cdot2MeOH$ reveals six different superexchange pathways (Scheme 4), the presence of the pentacoordinate $Ni^{II}$ cation (Ni12) being the main source of such a lack of symmetry. Thus, at first sight, modeling the magnetic data for $7\cdot4.75H_2O\cdot2MeOH$ appears quite complicated, due to the high number of magnetic variables. However, it is well know that DFT calculations can give a good estimation of the exchange coupling constants, and for this reason,

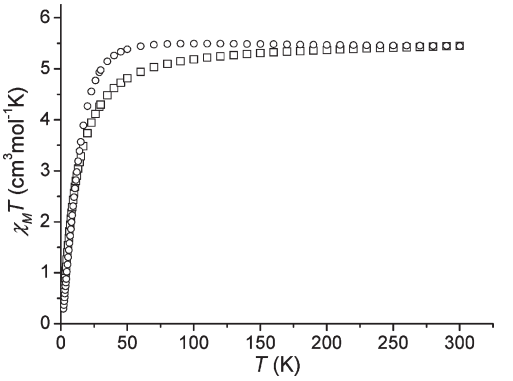


**Figure 9.** Experimental $\chi_M T$ versus $T$ product (□) for $7\cdot4.75H_2O\cdot2MeOH$ in comparison with that obtained from the DFT calculated $J$ values (○).

theoretical studies were performed in order to try to interpret the experimental magnetic behavior.

Accordingly, six $J$ values (see Computational Details section) were considered for the DFT study of this complex. This yields the following calculated $J$ values: $2J_1 = +11.6$ cm$^{-1}$, $2J_2 = +10.7$ cm$^{-1}$, $2J_{3a} = +0.54$ cm$^{-1}$, $2J_{3b} = +1.3$ cm$^{-1}$, $2J_{4a} = -4.03$ cm$^{-1}$, and $2J_{4b} = -11.2$ cm$^{-1}$. Thus, the two exchange couplings within the binuclear units (**7a** and **7b**) are ferromagnetic, while the interbinuclear interactions are rather weak, with the exception of the $J_{4a}$ and $J_{4b}$ values that are the responsibility of the decay of the $\chi_M T$ curve at low temperatures. These interactions correspond to the anti−anti and syn−anti exchange pathways of the carbonato bridge, respectively, and their sign (antiferromagnetic anti−anti and ferromagnetic syn−anti) resembles the behavior of carboxylate donors.[39]

The accuracy of these calculated $J$ values can be checked in Figure 9, by comparison of the curve obtained from such DFT $J$ values with the experimental one. This comparison shows a good agreement of both sets of data, considering the high sensitivity of the curve with small changes in the $J$ values.[40] Probably, the strength of the antiferromagnetic interactions is slightly underestimated in the calculated $J$ values, and the decay in the theoretical curve starts at low temperatures.

It is worth noting that the interactions where the pentacoordinate Ni12 cation is involved show a stronger coupling than the equivalent ones with only octahedral $Ni^{II}$ cations. The reason for such behavior can be easily understood taking into account a larger contribution of the orbitals of the bridging axial oxygen atom in the magnetic orbitals. Therefore, if the coupling is antiferromagnetic ($J_{4b}$), the predominant overlap term is larger, while for a ferromagnetic coupling ($J_{3b}$), the bielectronic integral should also be larger.

The presence of ferromagnetic exchange interactions within the binuclear units (**7a** and **7b**) has been explored in more detail. Usually, nature prefers antiferromagnetic interactions. Ferromagnetic couplings sometimes appear due to an unexpected degeneracy of the orbitals bearing the unpaired electrons, and consequently, to

(39) Rodríguez-Fortea, A.; Alemany, P.; Alvarez, S.; Ruiz, E. *Chem.—Eur. J.* **2001**, *7*, 627–637.
(40) Ruiz, E.; Cano, J.; Alvarez, S. *Chem.—Eur. J.* **2005**, *11*, 4767–4771.

**Table 5.** Calculated Exchange Coupling Constants $2J_1$ and $2J_2$ for **7**, Using the B3LYP Functional for Different Binuclear Models Changing the Number of Active Bridging Ligands

| | exchange pathway $2J_1$ |
|---|---|
| OCO, NCN, O (OPh) | +11.31(+11.63)[a] |
| OCO, O (OPh) | −17.81 |
| NCN, O (OPh) | +8.62 |
| | exchange pathway $2J_2$ |
| O ($\mu_2$-$CO_3^{2-}$), NCN, O (OPh) | +11.22(+10.65)[a] |
| O ($\mu_2$-$CO_3^{2-}$), O (OPh) | −12.48 |

[a] In parentheses are values corresponding to the whole tetranuclear complex

**Scheme 4.** Representation of the Different Superexchange Pathways for **7**

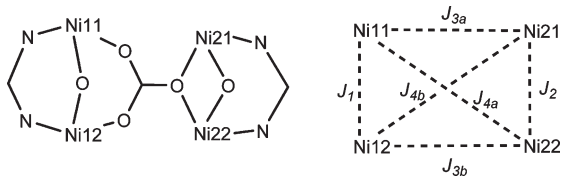


avoid the electronic repulsion, the system adopts a spin as high as possible. The degeneracy of the orbitals is in some cases provoked by the combination of bridging ligands with opposite shifts of the orbital energies (countercomplementarity effect).[41] Thus, the bridging ligands separately would cause antiferromagnetic couplings, but its combination results in degeneracy of the orbitals and ferromagnetism. Hence, we have performed some calculations using some binuclear models, by modifying the bridging ligands, in order to check the existence of the countercomplementarity effect.

The new $2J$ values obtained with these models (see Table 5) are very similar to those found for the whole tetranuclear complex. These results clearly indicate that in both cases ($2J_1$ and $2J_2$) the presence of the triple bridge results in a ferromagnetic coupling. However, the elimination of the central carbon atom of the imidazolidine bridge and the inclusion of hydrogen atoms to avoid dangling bonds give a new antiferromagnetic system. Accordingly, the presence of the NCN link plays a fundamental role in the observed ferromagnetic interactions within the binuclear units. This result, which seemed to be pointed out by the experimental data obtained for triple-bridged bis($\mu$-oxo)−$\mu$-NCN nickel complexes,[3c,5d,6d,7c] is now corroborated and extended to nickel compounds bearing $\mu$-oxo−$\mu$-NCN−$\mu$-OCO joints.

The effect of the carbonato bridge in the magnetic interactions was also checked (Table 5), and it seems that its influence in the $2J_1$ coupling constant is relatively small. Consequently, the elimination of such a ligand does not significantly change the nature of the interaction. This small impact of the carbonato donors was also noticed in reported $Cu^{II}$ complexes with similar bridging ligands.[6c]

(41) Kahn, O. *Molecular Magnetism*; VCH Publishers, Inc.: New York, 1993.

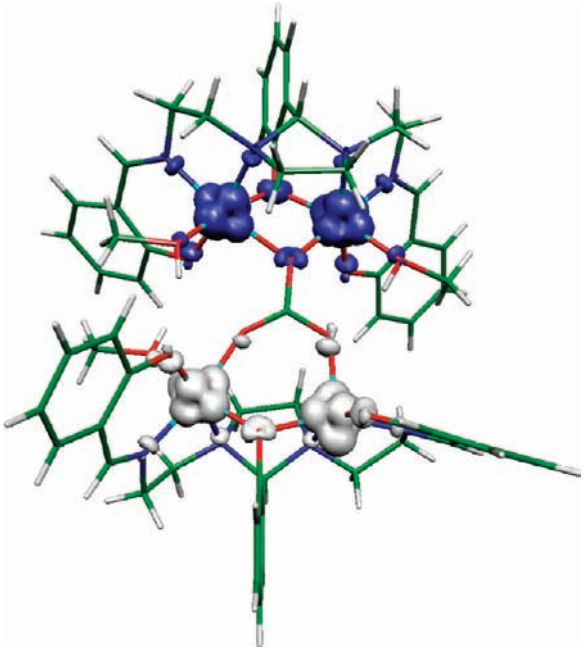

**Figure 10.** Representation of the spin density maps calculated at the B3LYP level for the $S = 0$ ground state of the tetranuclear complex **7**. Clear and dark regions indicate positive and negative spin populations (cutoff = 0.02 $e^-$/$bohr^3$), respectively.

Moreover, the spin density distribution for the ground state of **7** was analyzed, and it is shown in Figure 10. The M−L antibonding nature of the orbitals bearing the unpaired electrons causes the predominance of the delocalization mechanism over the spin polarization.[42,43] Thus, the sign of the spin densities of the atoms coordinated to the $Ni^{II}$ cations is the same as that of the metal ion. In the case of the pentacoordinate $Ni^{II}$ cation (Figure 10, right and below), the bigger spin density on the bridging oxygen atom of the carbonate ligand (O12) clearly indicates a larger participation of the orbitals of such an atom in the intrabinuclear exchange interactions in comparison with the other bridging oxygen atoms of the same binuclear unit.

Bearing in mind the $J$ values for **7** obtained by DFT calculations, several models were tested in order to try to explain the observed experimental magnetic behavior. In a first approach, some simplifications were pondered, in an attempt to avoid overparameterization. In this way, both syn−anti and both anti−anti superexchange pathways through the carbonate ligand were considered as equal, thus choosing a four-$J$ model (with $J_{3a} = J_{3b}$ and $J_{4a} = J_{4b}$ in Scheme 4). Consequently, the fitting with the MAGPACK program was performed with the mentioned four-$J$ model, introducing the $D_{Ni}$ and TIP parameters and restricting the $J$ values. The restrictions imposed were $J_1 > 0$, $J_2 > 0$, $J_3 > 0$, and $J_4 < 0$, in agreement with DFT results. It must be said that it was not possible to obtain a good match of the experimental $\chi_M T$ versus $T$ curve with this model.

(42) Cano, J.; Ruiz, E.; Alvarez, S.; Verdaguer, M. *Comments Inorg. Chem* **1998**, *20*, 27–56.

(43) Ruiz, E.; Cirera, J.; Alvarez, S. *Coord. Chem. Rev.* **2005**, *249*, 2649–2660.

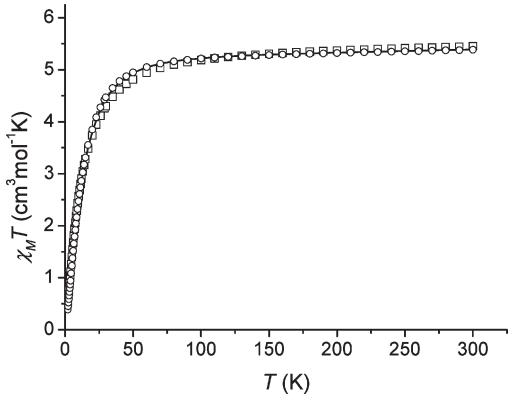


**Figure 11.** Plot of $\chi_M T$ versus $T$ for $7\cdot4.75H_2O\cdot2MeOH$. (□) Experimental data, (—) best fit without $D_{Ni}$, (○) best fit including $D_{Ni}$ (see text).

Accordingly, the magnetic data for $7\cdot4.75H_2O\cdot2MeOH$ were treated taking into account the six different superexchange pathways. On the basis of the theoretical calculations, some limits were imposed: $J_1 > 0$, $J_2 > 0$, $J_{3a} > 0$, $J_{3b} > 0$, $J_{4a} < 0$, and $J_{4b} < 0$ and TIP $= 6.0 \times 10^{-4}$ cm$^3$ mol$^{-1}$ (typical value for tetranuclear $Ni^{II}$ complexes in Oh or Sqp environments).[44,45] Thus, the best fit of the experimental data with the MAGPACK program using this six-$J$ model (Scheme 4) leads to the parameters $2J_1 = 11.02$ cm$^{-1}$, $2J_2 = 9.0$ cm$^{-1}$, $2J_{3a} = 1.40$ cm$^{-1}$, $2J_{3b} = 3.0$ cm$^{-1}$, $2J_{4a} = -2.40$ cm$^{-1}$, $2J_{4b} = -17.68$ cm$^{-1}$, and $g = 2.28$, with $R = 8.49 \times 10^{-5}$ (Figure 11). These values are in good agreement with those obtained from theoretical calculations.

In a third approximation, a new fit using the 6$J$ model with the mentioned restrictions and including the $D_{Ni}$ parameter was tried. This gives as best fitting parameters the following ones: $2J_1 = 10.20$ cm$^{-1}$, $2J_2 = 7.80$ cm$^{-1}$, $2J_{3a} = 1.80$ cm$^{-1}$, $2J_{3b} = 3.40$ cm$^{-1}$, $2J_{4a} = -2.60$ cm$^{-1}$, $2J_{4b} = -17.0$ cm$^{-1}$, $g = 2.28$, and $|D_{Ni}| = 5.6$ cm$^{-1}$, with $R = 1.12 \times 10^{-4}$ (Figure 11). The 2$J$ and $g$ values are quite similar to the previous calculated ones, and the introduction of the $D_{Ni}$ parameter leads to small changes in all of the coupling constants. Besides, the $|D_{Ni}|$ value is in the range of the expected ones.[38]

## Conclusions

Nickel(II) acetate/$H_3L$ is a versatile system that can yield a variety of complexes as a function of the reaction stoichiometry and of the pH of the medium. This paper summarizes the complicated reaction scheme of this system, rationalizing the different reaction patterns that allow isolation of the asymmetric binuclear $1\cdot3.25H_2O$, pentanuclear $2\cdot2.7H_2O\cdot1.5MeOH$, or trinuclear $3\cdot3H_2O\cdot0.5MeOH$ complexes versus the more symmetric binuclear $4\cdot1.75H_2O$, $5\cdot3H_2O\cdot1.5MeOH$, and $6\cdot H_2O\cdot3MeOH$ and tetranuclear $7\cdot4.75H_2O\cdot2MeOH$ compounds.

The newly characterized complexes $4\cdot1.75H_2O$ to $7\cdot4.75H_2O\cdot2MeOH$ show some outstanding structural features. In this way, it is remarkable that the $C_s$ symmetric complex $6\cdot H_2O\cdot3MeOH$ is chiral in the solid state due to an intramolecular H bond. Likewise, the crystal is homochiral, as it gives rise to homochiral helical chains formed by complex molecules and solvates, which are also joined by H bonds. Furthermore, $7\cdot4.75H_2O\cdot2MeOH$ presents two different geometries for the nickel ions, the Sqp arrangement being very uncommon for nickel complexes of this kind, and it exhibits a $\mu_4$ coordination mode for the carbonato ligand that has not been previously described for nickel complexes.

In addition, the magnetic characterization of $5\cdot3H_2O\cdot1.5MeOH$ to $7\cdot4.75H_2O\cdot2MeOH$ shows that the bis($\mu$-oxo)−$\mu$-NCN bridge provokes a ferromagnetic coupling. This result is further analyzed by DFT studies on $7\cdot4.75H_2O\cdot2MeOH$, which demonstrates that the NCN bridge is the cause of the ferromagnetic coupling transmited not only through a bis($\mu$-oxo)−$\mu$-NCN bridge but also through a $\mu$-oxo−$\mu$-NCN−$\mu$-OCO magnetic pathway. Thus, it seems that the presence of this kind of imidazolidine connection always promotes a parallel alignment of the unpaired electrons, independently of the nature of the additional bridges. And this is a remarkable end result, as there are not many ligands that show this intrinsic feature. In addition, the magnetic characterization of $7\cdot4.75H_2O\cdot2MeOH$ contributes to increasing the scarce number of coordination modes of the carbonate ligand magnetically analyzed for nickel complexes. This study shows that the magnetic interaction mediated by this $\mu_4$-$CO_3$ bridge presents two kinds of contributions operating in opposite directions.

**Acknowledgment.** The research reported here was supported by Xunta de Galicia (PGIDTIT06PXIB209043PR), Dirección General de Investigación del Ministerio de Educación y Ciencia (CTQ2008-06670-C02-01) and Comissió Interdepartamental de Ciència i Tecnologia (CIRIT, 2009SGR-1459). The computing resources were generously made available in the Centre de Supercomputació de Catalunya (CESCA) with a grant provided by Fundació Catalana per a la Recerca (FCR) and the Universitat de Barcelona.

**Supporting Information Available:** Plot of $\chi_M T$ versus $T$ for $6\cdot H_2O\cdot MeOH$ and X-ray crystallographic data in CIF format for $4\cdot1.75H_2O$, $5\cdot3H_2O$, $6\cdot H_2O\cdot3MeOH$, and $7\cdot4.75H_2O\cdot2MeOH$. This material is available free of charge via the Internet at http://pubs.acs.org.

(44) Clemente-Juan, J. M.; Chansou, B.; Donnadieu, B.; Tuchagues, J. P. *Inorg. Chem.* **2000**, *39*, 5515–5519.
(45) Pavlishchuk, V. V.; Kolotilov, S. V.; Addison, A. W.; Prusham, M. J.; Schollmeyer, D.; Thompson, L. K.; Goreshenik, E. A. *Angew. Chem., Int. Ed.* **2001**, *40*, 4734–4737.